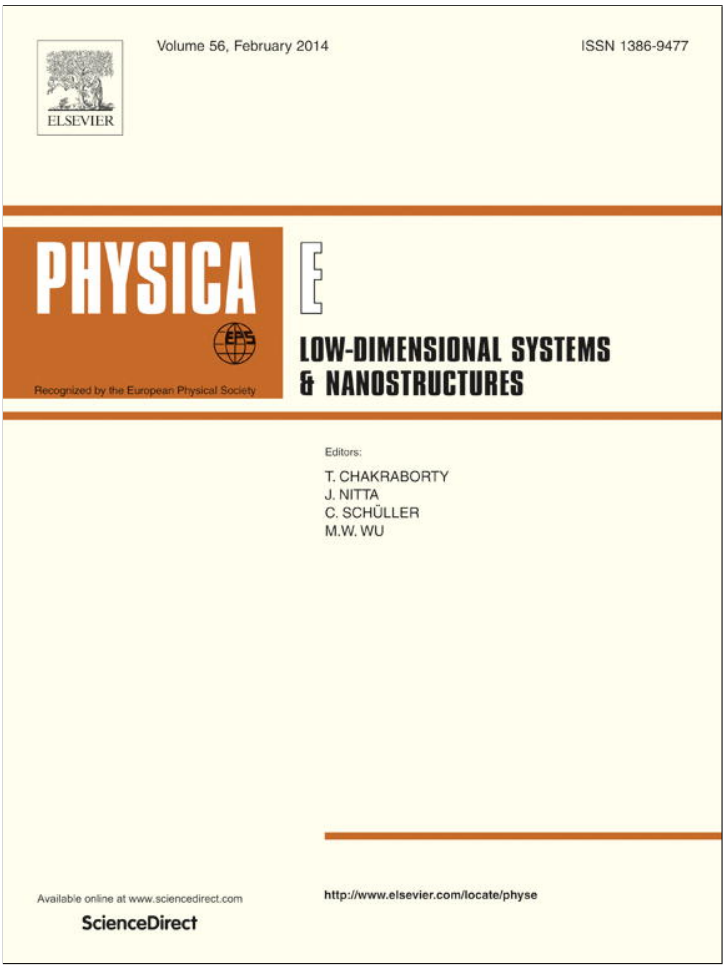

Physica E 56 (2014) 48–54

Contents lists available at ScienceDirect

Physica E

journal homepage: www.elsevier.com/locate/physe

Role of Defects on structural and electronic properties of zigzag C_3N nanotubes: A first-principle study

Seifollah Jalili [a,b,*], Farzad Molani [a], Mojdeh Akhavan [b], Jeremy Schofield [c]

[a] Department of Chemistry, K.N. Toosi University of Technology, P.O. Box 15875-4416, Tehran, Iran
[b] Computational Physical Sciences Research Laboratory, School of Nano-Science, Institute for Research in Fundamental Sciences (IPM), P.O. Box 19395-5531 Tehran, Iran
[c] Chemical Physics Theory Group, Department of Chemistry, University of Toronto, 80 Saint George Street, Toronto, Ontario, Canada M5S 3H6

HIGHLIGHTS

- Stone–Wales (SW) and vacancy defects in C_3N nanotubes were studied.
- The formation of SW defect in C_3N nanotubes is an endothermic process.
- Perfect and SW-defected tubes are semiconductors with direct band gap.
- Vacancy defects reconstruct to a 5–9 ring system with one dangling bond.
- The nanotubes with vacancy defects show ferromagnetic spin ordering.

ARTICLE INFO

Article history:
Received 10 February 2013
Received in revised form
5 June 2013
Accepted 29 July 2013
Available online 24 August 2013

Keywords:
C_3N nanotube
Stone–Wales defect
Vacancy defect
Density functional theory
Electronic property

ABSTRACT

The energetic, electronic, and structural properties of zigzag C_3N nanotubes with defects have been systematically investigated through the spin-polarized density-functional theory calculations. The four basic system types with Stone–Wales defects are characterized in terms of the defect stabilization energy and the band gaps. The most desirable bond rotation is related to a circumferential N–C bond. The role of vacancy defects on the above properties has been also investigated. Our results show that carbon vacancy is more favorable than nitrogen vacancy. Moreover, the electronic properties of the semiconducting C_3N nanotubes with defects have been studied using band structures and density of states plots.

1. Introduction

Carbon nanotubes (CNTs) hold great promise in a wide variety of electronic applications, including solar cells [1,2], sensors [3,4], batteries [5], and catalyst support materials [6]. Thus, modifying their electronic properties will have a potential impact on further application of CNTs in nano-electronics and optical devices. In order to achieve carbon nanotubes with different properties, doping is one of the methods. The studies on extrinsically doped CNTs have been reported [7,8]. Among all the doped CNTs, the N-doped CNTs are of special interest in both theoretical and applied studies [8,9]. Besides, doping CNTs through substitution of a carbon atom by a nitrogen atom results in one additional electron in the π-electron system. For instance when the extra electron is localized in semiconducting CNTs, the corresponding dopant state is a quasi-bound state [10]. Furthermore, carbon nitride nanotubes have attracted increasing interest due to their interesting electronic, chemical, and mechanical properties as well as large number of methods available for synthesis of carbon nitride compounds [11,12]. Also, these materials exhibit many interesting and useful mechanical properties such as high elastic recovery and low friction coefficient [13,14]. Thus, the study of replacing some of the carbon atoms in a CNT with nitrogen atoms seems to be necessary.

Multi-walled CN_x nanotubes are synthesized by pyrolyzing ferrocence/melamine mixture at 1050 °C in argon atmosphere [9]. Hales et al. [15] have recently studied structural and thermodynamic stability of small C_xN nanotubes with $x=1$, 2, 3, 5, and 7. They have shown that the C_3N nanotube exhibits a distorted structure that is

* Corresponding author at: Department of Chemistry, K.N. Toosi University of Technology, P.O. Box 15875-4416, Tehran, Iran. Tel.: +98 21 22853649; fax: +98 21 22853650.
E-mail addresses: sjalili@kntu.ac.ir (S. Jalili), fmolani@dena.kntu.ac.ir (F. Molani), m.akhavan@ipm.ir (M. Akhavan), jmschofi@chem.utoronto.ca (J. Schofield).

1386-9477/$ - see front matter © 2013 Elsevier B.V. All rights reserved.
http://dx.doi.org/10.1016/j.physe.2013.07.022

strongly independent of the chiral index [15]. Some predictions of the possible crystal structures for C_3N can be found in the literature [16,17]. Azevedo et al. [18] showed that C–N bonds are more favorable than the C–B bonds. As a result, the C_3N nanotube is more stable than the BC_3 one.

Nitrogen-doped CNTs have a more defective structure compared to undoped CNTs, with more disruptions in the graphitic lattice [19]. The vacancy defects (incomplete bonding defects) and the Stone–Wales (SW) defect [20] (a typical topological defect in the carbon nanostructures which is comprised of two pairs of five-membered and seven-membered rings) have been extensively studied in CNTs [21–23], boron-nitride nanotubes (BNNTs) [24], and BC_3 nanotubes [25].

In the present study, we have performed density functional theory (DFT) calculations on a (8,0) C_3N nanotube in order to investigate the role of SW defects, carbon vacancy (CV), and nitrogen vacancy (NV) on the structural, energetic, and electronic properties.

2. Computational details

Spin-polarized DFT calculations, implemented in the QUANTUM ESPRESSO package [26] were performed on (8,0) C_3N nanotubes. A plane-wave basis set with a cutoff value of 600 eV was used in combination with ultrasoft pseudo-potentials and the Perdew–Burke–Ernzerhof (PBE) [27] exchange-correlation functional within the generalized-gradient approximation (GGA). To determine the equilibrium structure of the systems, full relaxation without any constraints was performed until the forces acting on any atom are less than 0.001 eV/Å. The Brillouin-zone integration was performed with a $1\times1\times9$ Monkhorst–Pack k-points mesh [28]. A large supercell parameter of 20 Å was chosen in x and y directions to ensure negligible interaction between the system and its images in neighboring cells. Furthermore, we have measured the pyramidalization angles at selected atom sites using the Haddon's π-orbital axis vector (POAV) method [29].

3. Results and discussion

The optimized structures for five distinct atomic arrangements of C_3N nanotubes are shown in Fig. 1. Mazzoni and coworkers showed that, structures with phase-separated graphite islands should be favored in $B_xC_yN_z$ layered structures [30]. Having optimized and compared their total energies, we found that the structure A is the most stable among the others, which has a segregated graphite island-like while others lead to structures in which C, and N atoms are mixed. From now on, in the present study, this structure will be considered as the pristine structure. The role of Stone–Wales and vacancy defects has been investigated on the properties of the pristine nanotube. There are two distinct types of C−C and N−C bonds which are axial or circumferential with respect to the tube axis. As Table 1 shows, the axial and circumferential C−C bonds have equal lengths, while for the N−C bonds, circumferential bonds are longer than axial bonds.

3.1. Stone–Wales defects

Optimized structures for C_3N nanotubes including a SW defect are shown in Fig. 2. As a result of bond rotation by 90°, there are four kinds of SW defects for a zigzag C_3N nanotube. These are labeled as SW-NC-a, SW-CC-a, SW-NC-c, and SW-CC-c in Fig. 2. The local structure around the defect site for the four kinds of SW defects in C_3N nanotubes is compared with those of the pristine nanotube in Table 1.

The data listed in Table 1 reveal that the length of the central bond (the bond between atoms 1 and 2 in Fig. 2) for SW defect structures is considerably shorter than the corresponding bond of the pristine structure. The same behavior is also observed for CNT [21,31], and BNNT [21], but BC_3 [25] does not show such behavior. It is worth mentioning that the circumferential bond between atoms 1 and 2 in SW defect structures is shorter than the axial one which is exactly similar to what happens in the CNT [21,31], BNNT [32], and BC_3 [25] nanotubes.

The pyramidalization angle (θ_p) is a measure of the degree of sp^3 hybridization of an atom, defined as ($\theta_{\sigma p}-90^\circ$), where $\theta_{\sigma p}$ is the angle between σ and π bonds. For $\theta_p=0^\circ$, the hybrid is sp^2 as in a flat graphene [29,33] and for $\theta_p=19.5^\circ$ the atom is sp^3-hybridized as in methane. Recent computational studies have pointed out that the carbon atoms with high pyramidalization angles exhibit high reactivity [23,34,35]. The calculated θ_p for atoms 1 and 2 in Fig. 2, as compared to the values for the pristine tube, are presented in Table 1. Our results show that atoms 1 and 2 in

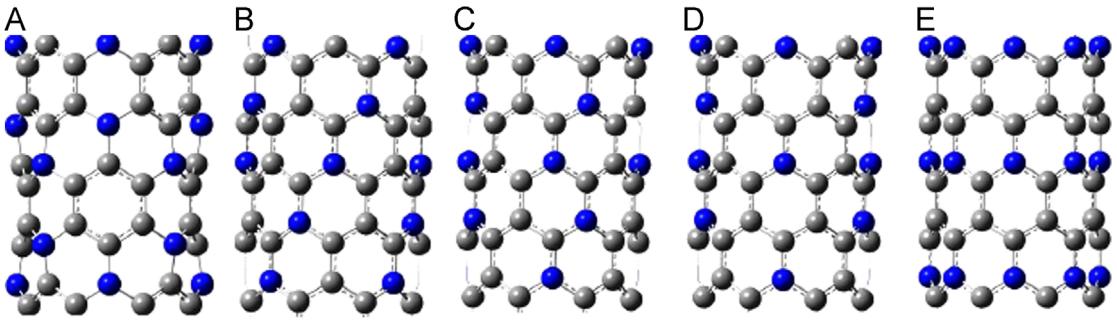

Fig. 1. Optimized structures of (8,0) C_3N nanotubes with different atomic arrangements. Gray and blue colors represent carbon and nitrogen atoms, respectively (For interpretation of the references to color in this figure legend, the reader is referred to the web version of this article).

Table 1
Structural and electronic properties of SW defects in C_3N nanotubes. The corresponding values for the defect-free nanotubes are given in parentheses.

System	Central bond length (Å)	Θ_p for 1, 2 atoms (deg.)	Formation energy (eV)	Energy gap (eV)
SW-NC-a	1.421 (1.427)	17.35 (13.84), 3.74 (2.65)	2.81	0.25
SW-CC-a	1.388 (1.416)	5.36 (4.53), 13.84 (4.52)	3.64	0.06
SW-CC-c	1.350 (1.416)	0.14 (2.65), 0.10 (4.56)	1.97	0.20
SW-NC-c	1.359 (1.450)	4.27 (13.84), 0.18 (4.56)	1.38	0.28

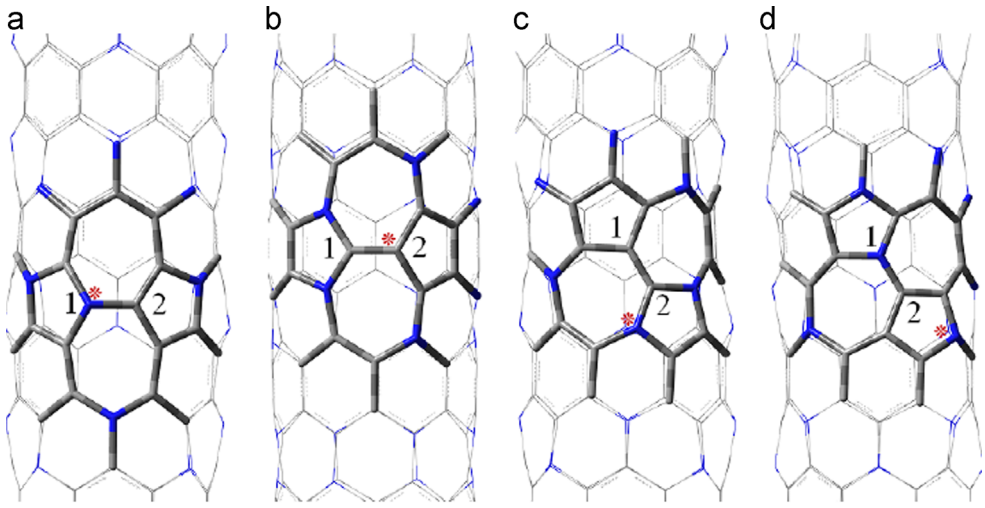

Fig. 2. Optimized structures for C_3N nanotubes with SW defects: (a) SW-NC-a, (b) SW-CC-a, (c) SW-CC-c, and (d) SW-NC-c. Atoms with the highest pyramidalization angle are showed by asterisks.

Table 2
Structural, energetic, and magnetic properties of atomic vacancy structures.

System	Length of new bonds (Å)	Total magnetization (μ_B)	Formation energy (eV)	Charge variation for dangling bond (e)
CV-1 db-5,9	1.421(C–C)	1.8	2.35	0.39
NV-3 db	–	2.0	4.79	0.18, 0.18, 0.13*
NV-3 db-deform	–	0.0	4.22	0.1, 0.35, 0.1*
NV-1 db-5,9	1.503 (C–C)	1.0	3.29	0.27

* For α, β, and γ atoms, respectively.

axial bond rotation (SW-NC-a and SW-CC-a) have a higher θ_p value with respect to the pristine nanotube, so atoms 1 and 2 move outward and a reactive site is localized on each of them. In other rotations (SW-CC-c and SW-NC-c), these atoms have a lower θ_p value with respect to the pristine nanotube. Hence, these atoms move inward and the reactive site is one atom or two atoms away from the 7–7 ring fusion. In fact, atoms with the highest θ_p, shown with asterisks in Fig. 2, can increase the bond length (steric hindrance). Despite the fact that nitrogen has a smaller covalent radius with respect to carbon, it prefers to have a high θ_p one atom or two atoms away from 7–7 ring fusion.

The formation energies for SW defects, which are defined as $E_f = E_{SW} - E_{pristine}$, are reported in Table 2. The positive formation energy means that the formation of these defects in C_3N is an endothermic process. The bond rotations in C_3N tubes, like CNTs [21,31] and BNNTs [32] have positive formation energies, but BC_3 [25] has negative energies in some rotations. Unlike the other structures, circumferential bond rotation is more stable than axial one in C_3N nanotube. To investigate the effect of the diameter on the stability of bond rotation, we studied (8,0), (10,0), and (12,0) nanotubes. Results showed that, this rule is observed for different diameters [21,25,31,32]. The formation energy as a function of tube diameter is shown in Fig. 3. Overall, the smaller the diameter of the nanotube with a SW defect has the lower the formation energy of the system. It can be concluded that the SW defect occurs preferentially in the smaller-sized C_3N nanotube. Furthermore, the formation energy difference between circumferential and axial SW defects decreases as the diameter of the CNT, BNNT, and SiCNT becomes larger [36–40]. Unlike BNNTs [32], the SW defect in a C_3N nanotube does not form unstable homo-elemental N–N bonds, and as a result, the structures are more stable. In N–C bond rotation the length of the bond shared by two heptagons (the

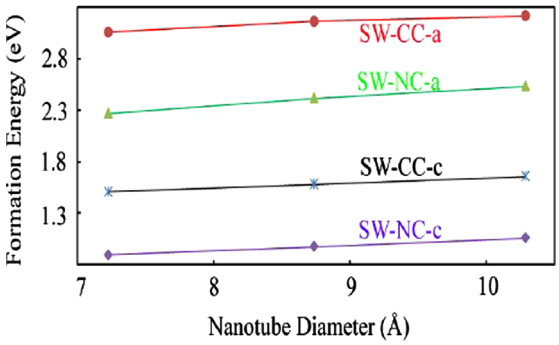

Fig. 3. Formation energy as a function of diameter for C_3N nanotubes for different atom bonds and rotation types.

central bond) is more than C–C one. As a result of increasing bond length, bond angles of atoms which are involved in 7–7 ring fusion are more than before. It means that, "steric hindrance" decreases as the bond length of the ring fusion becomes larger. With these descriptions and computational results, N–C bond rotation was more favorable than C–C bond rotation. Also, the SW-NC-c structure is the most stable C_3N nanotube, with the lowest formation energy and minimum structural deformation with respect to the defect-free C_3N nanotube. The stability order of four classes of SW defect structures is: SW-NC-c > SW-CC-c > SW-NC-a > SW-CC-a. Therefore, the direction of bond rotation is more significant than the type of atoms which makes the bond.

The electronic band structures of the pristine C_3N nanotube and the structures with SW defects are displayed in Fig. 4 and the values of energy gap are listed in Table 1. Defective structures remain semiconductor with a direct band gap. The energy gap for

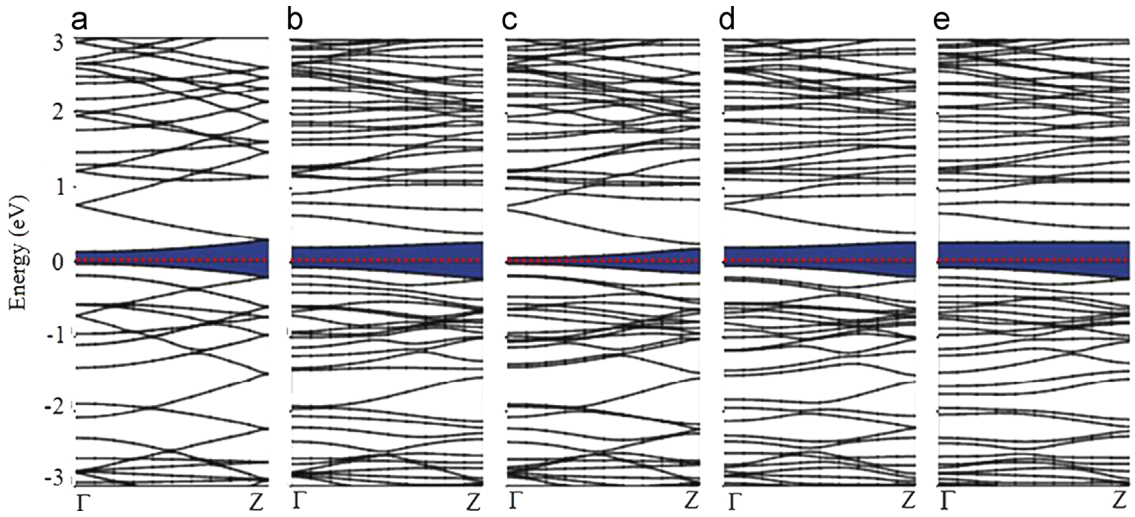

Fig. 4. Electronic band structures along the high symmetry direction of the Brillouin zone for the (a) defect-free (8,0) C_3N nanotube, (b) SW-NC-a, (c) SW-CC-a, (d) SW-CC-c, and (e) SW-NC-c. The gap between valence and conduction bands is distinguished by dark blue color. The dashed line indicates the position of the Fermi level, which is set to zero energy (For interpretation of the references to color in this figure legend, the reader is referred to the web version of this article).

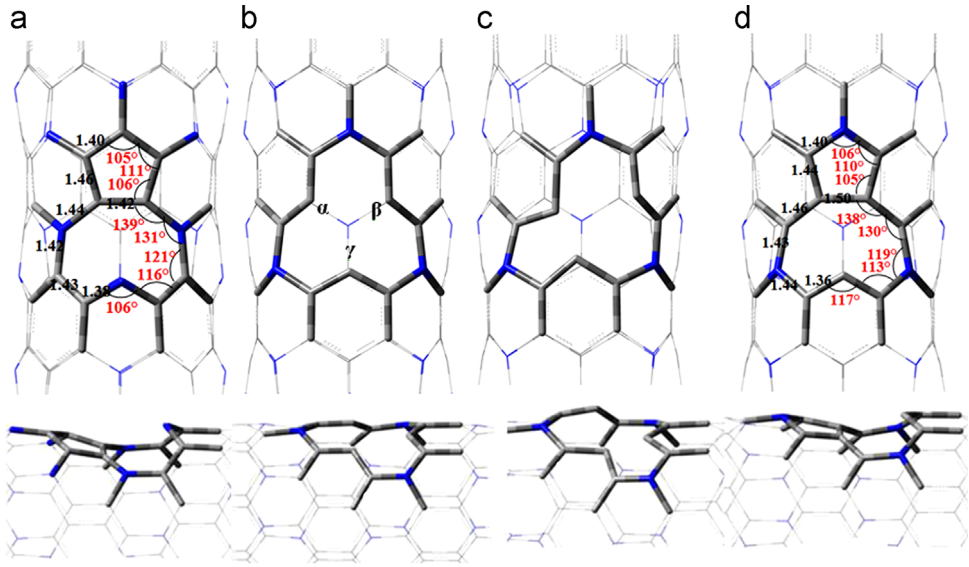

Fig. 5. Optimized structures for C_3N nanotubes with vacancies. (a) The most stable structure for carbon vacancy (CV-1 db-5,9); (b) the meta-stable structure for nitrogen vacancy (NV-3 db); (c) another meta-stable structure for nitrogen vacancy (NV-3 db-deform); and (d) the most stable structure for nitrogen vacancy (NV-1 db-5,9). Under-coordinated atoms are shown by α, β, and γ. Bond lengths and angles are presented for the most stable structures.

the pristine nanotube is 0.14 eV and increases as a result of SW defects, except for SW-CC-a system. Considering the energy gaps, it seems that the effect of bond rotation type in the energy gap does not follow a specific pattern. In addition, structures with a C–C bond at 7–7 ring fusion have a lower energy gap in comparison with the structures with a N–C bond. Compared to the defect-free tube, the structures with a N–C bond at 7–7 ring fusion cause the originally degenerate states to be split due to the breakage of nanotube symmetry. Furthermore, no "defect state" is observed near valance or conduction bands in band structures. As a result, the energy gap order is SW-NC-c > SW-NC-a > SW-CC-c > defect-free C_3N > SW-CC-a.

3.2. Vacancy defects

When a single atom is removed from the C_3N nanotube sidewall, unconstrained structure optimization leads to the formation of a new bond, perpendicular to the tube axis and the system is reconstructed to a five-membered and a nine-membered ring with a dangling bond or under-coordinated atom around the local defect region. In Fig. 5, these atoms are shown by α, β, and γ. Many initial structures were considered so that the final structures could be guaranteed. The most stable structure of CV defect with one dangling bond and five and nine membered rings (CV-1 db-5,9) is depicted in Fig. 5a. Although CV does not have a meta-stable structure, two meta-stable structures for NV are observed. One of them has three dangling bonds (NV-3 db) and the other one has three dangling bonds in which β atom moves slightly outwards (NV-3 db-deform). These metastable structures are shown in Fig. 5b and c, respectively. Fig. 5d shows the most stable NV-defected tube which has only one dangling bond and a new C–C bond to construct five and nine membered rings (NV-1 db-5,9). The bond lengths and angles of the most stable defective structures are exhibited in Fig. 5. Our results show that the new bond is always perpendicular to the tube axis and occurs between unsaturated carbon atoms. Comparing CV-1 db-5,9 with NV-1 db-5,9, it is seen that the new bond in NV defect is longer than that of the CV defect. Also, the unsaturated nitrogen atom in CV defect is more outward than the unsaturated carbon atom in CV defect.

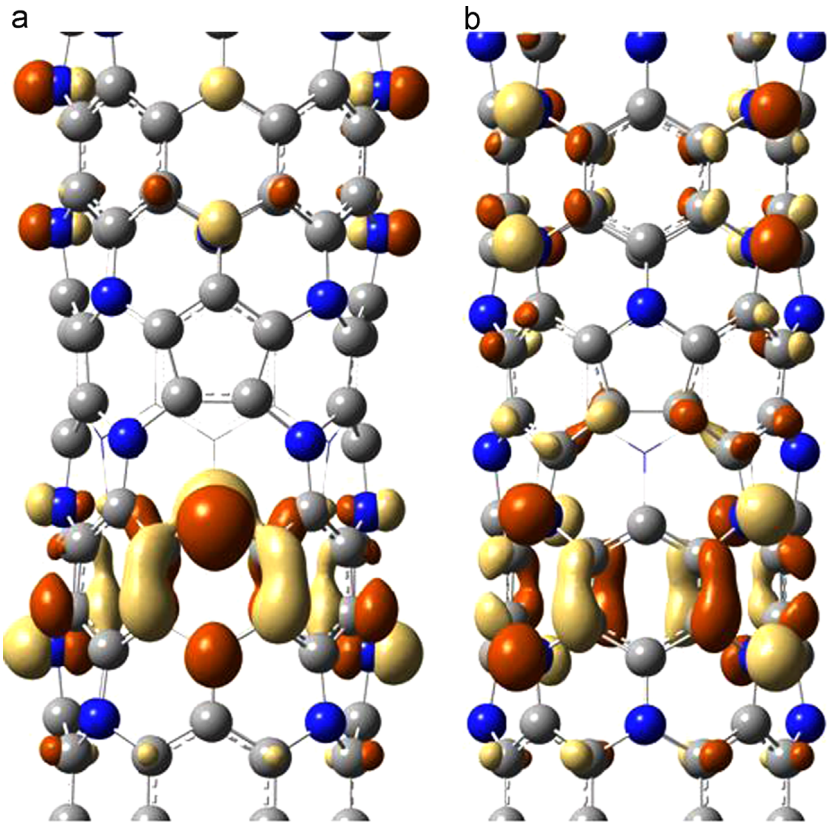

Fig. 6. Spin-density isosurfaces for (a) CV-1 db-5,9 and (b) NV-1 db-5,9. Brown and golden regions correspond to negative and positive polarization, respectively. The isodensity value is 0.001 μB/bohr^3 (For interpretation of the references to color in this figure legend, the reader is referred to the web version of this article).

For vacancies, defect formation energy is calculated from the energies of defected and pristine structures by $E_f = E_{defected} + \mu_X - E_{pristine}$, where μ_X is the chemical potential of carbon in a pure carbon nanotube or nitrogen in a gaseous N_2 molecule. This energy is reported for various vacancy defects in Table 2. One reason for such high defect formation energy is the dangling bond left at the atomic site γ after the reconstruction. Our results show that CV defect has a lower formation energy than NV defect. The most stable NV defect has 7.3 and 11.8 meV/atom lower formation energy than NV-3 db-deform and NV-3 db, respectively.

The net magnetic moments for vacancy structures are listed in Table 2. Due to the presence of dangling bonds, the stable structures show ferromagnetic ordering. In carbon vacancy, the under-coordinated atom moves drastically outward. Therefore, the hybridization between the dangling bond and other atoms is prohibited. Because there are three dangling bonds in NV-3 db, it has a high value of net magnetic moment. The average distance between three under-coordinated atoms in NV-3 db and NV-3 db-deform is 2.58 and 2.37 Å, respectively. As a result, dangling bonds in NV-3 db-deform can hybridize with each other and their neighboring atoms, showing paramagnetic ordering. In NV-1 db-5,9, carbon atom is unsaturated and moved slightly outward, resulting in a net magnetic moment of 1.0 μ_B. Clearly, the magnetism is due to the dangling bonds which have a localized unpaired spin, as shown in Fig. 6. The lower-energy structures of CV-1 db-5,9 and NV-1 db,5,9 have magnetic moments of 1.8 and 1.0 μ_B, respectively. The calculated charge variations (ΔQ) of under-coordinated atom (UA) for vacancy defect systems obtained by Löwdin charge analysis are listed in Table 2. It is noteworthy that a positive value for ΔQ indicates that the UA gains electron density. In CV-1 db-5,9, UA is nitrogen which is more electronegative than carbon in NV-1-db-5,9. Furthermore, when a carbon (nitrogen) is removed four (three) electrons can be free. So, nitrogen has more

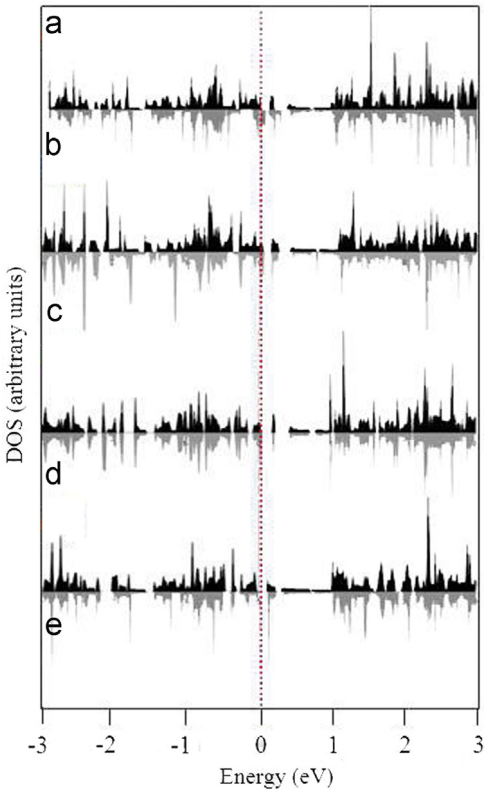

Fig. 7. Total density of state for (a) CV-1 db-5,9; (b) NV-3 db; (c) NV-3 db-deform; and (d) NV-1 db-5,9. Black and gray regions correspond to majority and minority spin configurations, respectively. The dashed red line indicates the position of the Fermi level, which is set to zero energy (For interpretation of the references to color in this figure legend, the reader is referred to the web version of this article).

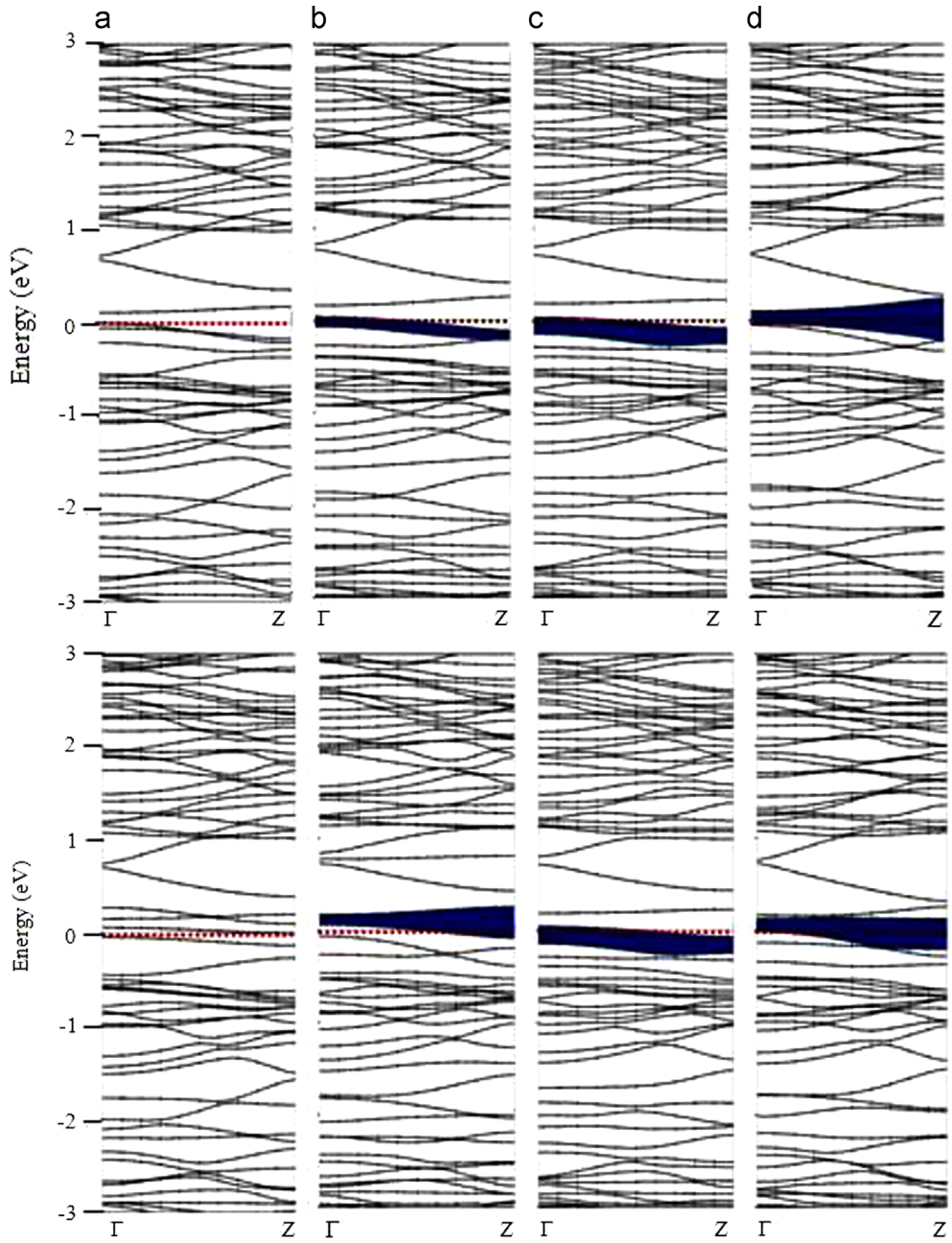

Fig. 8. Electronic band structures for (a) CV-1 db-5,9; (b) NV-3 db; (c) NV-3 db-deform; and (d) NV-1 db-5,9. The gap between valence and conduction bands is distinguished by dark blue color. Upper and lower panels correspond to majority and minority spin configurations. The dashed line indicates the position of the Fermi level, which is set to zero energy (For interpretation of the references to color in this figure legend, the reader is referred to the web version of this article).

charge density in comparison with the other atoms, depicted in Fig. 6.

The band structures and density of states of the vacancy systems have been determined and the results are compared with defect-free nanotube. In CV system, pentagon and nonagon introduced two "defect states" between valance and conduction bands. As shown in Figs. 7a and 8a, the gap between valance and conduction bands has disappeared and the system becomes metallic. Also, a defect state is observed for NV-3 db and NV-3 db-deform above and below the conduction band, respectively (Fig. 8b and c). There is no specific spin-up defect state for NV-1 db-5,9 but spin-down band structure shows a defect state below the conduction band which reduces the band gap. As a result, atomic imperfections in the C_3N nanotube play a crucial role in determining their electronic properties near the Fermi level.

4. Conclusions

In conclusion, through the first-principle DFT method, the structural and electronic properties of (8,0) C_3N nanotubes with defects were studied. Our calculations on Stone–Wales defect showed that, bond rotation in C_3N nanotube is an endothermic reaction and circumferential bond rotation is more favorable than the axial one. Also, N–C bond rotation was more favorable than C–C bond rotation. Stone–Wales defective structures remain semiconductor with a direct band gap. Structures with a C–C bond at 7–7 ring fusion in comparison with N–C bond has lower energy gap. Our results showed that, the carbon vacancy defect is more favorable than the nitrogen vacancy. Furthermore, the stable structures in vacancy defects showed ferromagnetic behavior. In addition, the most stable structure of carbon vacancy was metallic,

whereas the most stable structure for nitrogen vacancy was semiconductor.

Acknowledgments

Computations were performed on the GPC supercomputer at the SciNet HPC Consortium. SciNet is funded by: the Canada Foundation for Innovation under the auspices of Compute Canada; the Government of Ontario; Ontario Research Fund – Research Excellence; and the University of Toronto.

References

[1] M.W. Rowell, M.A. Topinka, M.D. McGehee, H.J. Prall, G. Dennler, N.S. Sariciftci, L. Hu, G. Gruner, Applied Physics Letters 88 (2006) 233506.
[2] J.E. Trancik, S.C. Barton, J. Hone, Nano Letters 8 (2008) 982.
[3] R. Antonov, A. Johnson, Physical Review Letters 83 (1999) 3274.
[4] M. Terrones, H. Terrones, F. Banhart, J.C. Charlier, P. Ajayan, Science 288 (2000) 1226.
[5] M. Morita, T. Hanada, H. Tsutsumi, Y. Matsuda, M. Kawaguchi, Journal of The Electrochemical Society 139 (1992) 1227.
[6] S.W. Bian, Z. Ma, W.G. Song, The Journal of Physical Chemistry C 113 (2009) 8668.
[7] M. Endo, H. Muramatsu, T. Hayashi, Y.A. Kim, G. Van Lier, J.C. Charlier, H. Terrones, M. Terrones, M.S. Dresselhaus, Nano Letters 5 (2005) 1099.
[8] Y. Ma, A. Foster, A. Krasheninnikov, R. Nieminen, Physical Review B 72 (2005) 205416.
[9] R. Czerw, M. Terrones, J.C. Charlier, X. Blase, B. Foley, R. Kamalakaran, N. Grobert, H. Terrones, D. Tekleab, P. Ajayan, Nano Letters 1 (2001) 457.
[10] Iann C. Gerber, Pascal Puech, Anis Gannouni, W. Bacsa, Physical Review B 79 (2009) 75423.
[11] C. Li, E.T. Thostenson, T.W. Chou, Composites Science and Technology 68 (2008) 1227.
[12] Javad Beheshtiana, Mohammad T. Baeib, Zargham Bagheric, A.A. Peyghand, Applied Surface Science 264 (2013) 699.
[13] T. Berlind, N. Hellgren, M.P. Johansson, L. Hultman, Surface and Coatings Technology 141 (2001) 145.
[14] J. Houska, M.M.M. Bilek, O. Warschkow, D.R. McKenzie, J. Vlcek, Physical Review B 72 (2005) 54204.
[15] J. Hales, A.S. Barnard, Journal of Physics: Condensed Matter 21 (2009) 144203.
[16] E. Kim, C. Chen, T. Köhler, M. Elstner, T. Frauenheim, Physical Review B 64 (2001) 094107.
[17] É. Sandré, C.J. Pickard, C. Colliex, Chemical Physics Letters 325 (2000) 53.
[18] S. Azevedo, R. De Paiva, Europhysics Letters 75 (2006) 126.
[19] S. Maldonado, S. Morin, K.J. Stevenson, Carbon 44 (2006) 1429.
[20] A.J. Stone, D.J. Wales, Chemical Physics Letters 128 (1986) 501.
[21] B.C. Pan, W.S. Yang, J. Yang, Physical Review B 62 (2000) 12652.
[22] W. Orellana, P. Fuentealba, Surface Science 600 (2006) 4305.
[23] H.F. Bettinger, The Journal of Physical Chemistry B 109 (2005) 6922.
[24] W. An, X. Wu, J. Yang, X. Zeng, The Journal of Physical Chemistry C 111 (2007) 14105.
[25] S. Jalili, M. Akhavan, J. Schofield, The Journal of Physical Chemistry C 116 (2012) 13225.
[26] P. Giannozzi, S. Baroni, N. Bonini, M. Calandra, R. Car, C. Cavazzoni, D. Ceresoli, G.L. Chiarotti, M. Cococcioni, I. Dabo, Journal of Physics: Condensed Matter 21 (2009) 395502.
[27] J.P. Perdew, K. Burke, M. Ernzerhof, Physical Review Letters 77 (1996) 3865.
[28] H.J. Monkhorst, J.D. Pack, Physical Review B 13 (1976) 5188.
[29] R. Haddon, The Journal of Physical Chemistry A 105 (2001) 4164.
[30] M.S. Mazzoni, R. Nunes, S. Azevedo, H. Chacham, Physical Review B 73 (2006) 073108.
[31] T.C. Dinadayalane, J. Leszczynski, Chemical Physics Letters 434 (2007) 86.
[32] Y. Li, Z. Zhou, D. Golberg, Y. Bando, P. von Ragué Schleyer, Z. Chen, The Journal of Physical Chemistry C 112 (2008) 1365.
[33] R. Haddon, Journal of the American Chemical Society 112 (1990) 3385.
[34] T. Lin, Wei-De Zhang, J. Huang, C. He, The Journal of Physical Chemistry B 109 (2005) 13755.
[35] X. Lu, Z. Chen, P.v.R. Schleyer, Journal of the American Chemical Society 127 (2005) 20.
[36] W.H. Moon, H.J. Hwang, Physica E: Low-dimensional Systems and Nanostructures 28 (2005) 419.
[37] Z. Wang, F. Gao, J. Li, X. Zu, W.J. Weber, Journal of Applied Physics 106 (2009) 084305.
[38] A. Krasheninnikov, F. Banhart, J. Li, A. Foster, R. Nieminen, Physical Review B 72 (2005) 125428.
[39] L. Zhou, S.-Q. Shi, Applied Physics Letters 83 (2003) 1222.
[40] B. Akdim, T. Kar, X. Duan, R. Pachter, Chemical Physics Letters 445 (2007) 281.